PERGAMON

Available online at www.sciencedirect.com

SCIENCE DIRECT®

Corrosion Science 45 (2003) 2563–2575

CORROSION SCIENCE

www.elsevier.com/locate/corsci

# On the akaganéite crystal structure, phase transformations and possible role in post-excavational corrosion of iron artifacts

Kenny Ståhl [a,*], Kurt Nielsen [a], Jianzhong Jiang [b], Bente Lebech [c], Jonathan C. Hanson [d], Poul Norby [d], Jettie van Lanschot [e]

[a] *Department of Chemistry, Technical University of Denmark, DK-2800 Lyngby, Denmark*
[b] *Department of Physics, Technical University of Denmark, DK-2800 Lyngby, Denmark*
[c] *Condensed Matter Physics and Chemistry Department, Risø National Laboratory, DK-4000 Roskilde, Denmark*
[d] *Chemistry Department, Brookhaven National Laboratory, Upton, NY 11973, USA*
[e] *School of Conservation, Esplanaden 34, DK-1263 Copenhagen, Denmark*

Received 6 November 2002; accepted 4 March 2003

**Abstract**

The crystal structure of akaganéite and the akaganéite to hematite transition has been studied by means of conventional and synchrotron X-ray and neutron powder diffraction. The chemical formula of akaganéite can be written as $FeO_{0.833}(OH)_{1.167}Cl_{0.167}$. The crystal structure does not contain free water. Heating below 200 °C will not alter the akaganéite structure. Initial water loss can be attributed to a large amount of adsorbed water due to a very small particle size; 0.15 μm by 0.03 μm. Chloride is released from the structure only in connection with the transformation to hematite. Due to its stability, the presence of akaganéite does not in itself posses a threat to iron artifacts, but it is rather a symptom of the presence of high concentrations of chloride in an acidic environment.


*Keywords:* Archaeological iron; B. XRD; B. Mössbauer spectroscopy; C. Exfoliation corrosion

* Corresponding author. Tel.: +45-45-252019; fax: +45-45-883136.
*E-mail address:* kenny@kemi.dtu.dk (K. Ståhl).

0010-938X/$ - see front matter © 2003 Elsevier Ltd. All rights reserved.
doi:10.1016/S0010-938X(03)00078-7

## 1. Introduction

*Archaeology/conservation*. For many years the stabilization of archaeological iron has presented serious problems for conservators. The deterioration of archaeological iron has been described thoroughly. Although there seems to be a general agreement on the corrosion products formed, the exact role of chloride and the exact structure of chloride-containing corrosion products is still under discussion [1–4]. The initial corrosion product of iron consists of ferrous ions, which form a variety of insoluble corrosion products by further reaction with the hydroxide ion produced at the cathode or other species in the environment. The corrosion layer is typically built up by a magnetite layer (lower oxygen levels) near the metal core, covered by a layer of ferric oxide (higher oxygen levels), typically goethite, cemented with soil particles. During burial, the porous oxide layer is filled with an aqueous electrolyte containing a large amount of ferrous ions. Hydrolysis of ferrous ions lowers the pH, and chloride ions will in most cases be the dominant counter ion due its to high mobility and availability. When artifacts are excavated, the ferrous ions oxides, which lower the pH even more. The low pH at the iron surface can only be explained through the separation of the cathodic and anodic corrosion reactions. Measurements of pH and $E$ (potential) on marine finds have shown a relatively acidic and reducing environment in contact with the corroding iron [3]. Even at modest relative humidity, oxidation may result in weeping, i.e. showing yellow droplets containing ferrous and ferric ions on the surface of the artifacts [1,2,4]. Formation of ferric oxyhydroxides is associated with a volume expansion, which cause cracks and exfoliation of the corrosion layers or the whole artifact, which in turn may accelerate the deterioration. At the position of fracture, an orange powder can be observed, which on several artifacts has been identified as β-FeOOH, akaganéite [1,4,5]. Thus the local high concentration of chloride combined with a low pH is favourable for akaganéite formation and makes akaganéite of special relevance to the stability of archaeological objects. Conservators have been using various treatments for removal of chlorides from artifacts including different desalination and heating treatments. The large body of work has however not provided a clear consensus about a preferred treatment. The deteriorating role of chlorides is still discussed. It may be indirect as a counter ion to the unstable ferrous ion and hydrogen as well as it decreases the critical relative humidity or it may participate in a corrosion cycle, as proposed by Askey [6]. Heating at high temperature can cause irreversible loss of potential metallurgical information. Cold-worked iron will begin to recrystallize at the annealing temperature (500 °C) while quenched steels hardly tolerate more than 100 °C [7]. Volatilisation of chlorides requires temperatures between 400 and 700 °C dependant of choice of gas [8]. Recently low-pressure hydrogen plasma has been used in metal conservation. Investigation of the critical temperature and treatment time resulted in a treatment temperature of 300–400 °C for eight days to remove all chlorides [9,10] The current status is low pressure plasma treatment at 120 °C to decrease the density of the corrosion layer followed by an alkaline desalination [11].

Desalination treatments, including alkaline and de-aerated solutions, tend to extend the period before they recorrode, but there is a large scatter in the results,

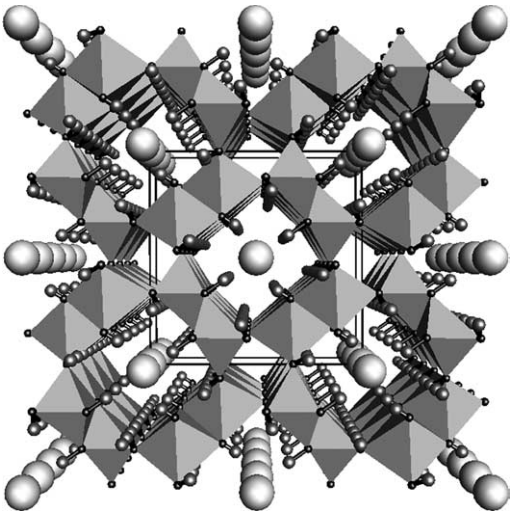

Fig. 1. The crystal structure of akaganéite shown viewed down the *b*-axis. Large spheres represent chlorides, small terminal spheres hydrogens.

although there is a good differentiation between the treatments investigated the alkaline treatment being superior to the neutral solutions [12–15]. It has previous been shown that β-FeOOH releases chlorides in solutions with pH > 7 until a chloride content of 2–3% in the solid is reached. If further extraction is needed it will involve a phase transformation [3].

*Crystallography*. Akaganéite, β-FeOOH, was first recognized by Weiser and Milligan [16], who uniquely distinguished it from other members of the Fe–O–H–Cl system by means of powder diffraction. The crystal structure of β-FeOOH was shown by Mackay [17] to be related to the hollandite structure, although with chloride anions in the channels. Mackay [18] also showed that β-FeOOH is identical to the mineral akaganéite. The first structure refinement was carried out by Post and Buchwald [19], who demonstrated that akaganéite has a monoclinic crystal structure with space group I2/m, $a = 10.600$, $b = 3.0339$, $c = 10.513$ Å and $\beta = 90.24°$. The crystal structure projected down the *b*-axis is shown in Fig. 1.

*Transformations*. There are several reports on phases in the Fe–O–H–Cl system into which akaganéite can be transformed, for example FeOCl, α-FeOOH (goethite) and $Fe_2O_3$ (hematite). Hematite is the thermodynamically most stable of these phases, and being chloride free and with low specific volume, it could be the preferred end product from an akaganéite transformation from a conservational point of view. However, the main purpose for conservation of archaeological iron is to treat and/or stabilize all or part of the corrosion products as it represents the actual shape of the artifact.

The aim of the present investigation was to establish the role of akaganéite in post-excavational corrosion by

- firmly establish the crystal structure of akaganéite including correct positions of chloride ions and hydrogens,
- study of the effects of the chloride contents on mild heating, where
- thermogravimetry have shown significant weight loss,
- study the akaganéite to hematite reaction in situ, possibly to detect intermediate phases involved in the transformation,

so as to provide a basis for further development or assessment of possible treatment methods.

## 2. Experimental methods

*Preparations*. Akaganéite was prepared by heating 0.2 M $FeCl_3$ solutions to 353 K for 5 h. The solutions were made from anhydrous $FeCl_3$ and $H_2O$ or $D_2O$. They will in the following be referred to as H-akaganéite and D-akaganéite, respectively. The brown crystalline precipitate was washed with water until the filtrate was chloride-free, and dried in air for 24 h at 343 K. The phase purity of the samples was confirmed by X-ray powder diffraction.

*Conventional X-ray powder diffraction*. The conventional X-ray powder diffraction data sets were collected using a Philips PW1820/3711 diffractometer and CuK$\alpha$ radiation. The diffraction patterns were accumulated in the $2\theta$-range 5–130° in steps of 0.02° spending 10 s/step. The intensity data were corrected for the effects of the auto-divergence slit.

*In situ synchrotron X-ray powder diffraction*. Synchrotron data were collected at beamline X7B, NSLS, at Brookhaven National Laboratory, USA. The method employed a moving imaging plate as described by Norby [20]. The sample was contained in a glass capillary and heated to 200 °C during 5 h and then kept at 200 °C for another 5 h, while the powder pattern was recorded on a continuously moving imaging plate. The imaging plate data was then split up in twenty separate data sets, corrected and converted into equal 2°-steps before structure refinements. The wavelength used was 0.96104 Å.

*Neutron powder diffraction*. The neutron data sets were collected at the TAS-III beamline at the Risø National Laboratory, Denmark. To increase the scattered intensity, the data collections were performed without the primary beam collimator. The wavelength used was 1.54172 Å, obtained with a Ge(5 1 1) monochromator.

*Crystal structure refinements*. The crystal structures were refined from powder diffraction data using the Rietveld method with a local modification of the LHMP1 program [21]. The Fe sites were modelled with coupled anisotropic temperature factors, while all other sites were modelled with isotropic temperature factors. All coordinates except those for Cl and two partially occupied hydrogen positions, H2 and H4, were refined. The *y*-coordinate for Cl was fixed to 0.11 as discussed below.

*Thermogravimetric (TG) and mass spectrometric (MS) analysis*. The TG analyses were performed on a Mettler TA1-LT using a heating rate of 2 K/min in a dry

airflow of 50 ml/min. The TG outlet was connected to a Fison, VG Quadropoles mass spectrometer recording the oxygen and chlorine related signals.

*Mössbauer spectroscopy*. Mössbauer spectroscopy was carried out with a conventional constant-acceleration spectrometer in transmission geometry with a source of about 25 mCi 57Co in an Rh-matrix. All isomer shifts were measured relative to that of α-Fe at room temperature. A closed-cycle helium cryostat was used for the low-temperature measurements.

## 3. Results

*Crystal structure*. The crystal structure refinements from conventional and synchrotron X-rays as well as neutron powder diffraction data all confirm the general features of the akaganéite structure as described by Post and Buchwald [19]. However, there are two remaining problems in that description: The chlorine occupancy and the charge balancing of the structure. With Cl placed in (0,0,0) the Cl–Cl distance will be equal to the *b*-axis length, i.e. 3.0 Å, which is much less than two times the ionic radius of 3.6 Å for Cl. In effect, only every second Cl site could be populated. The refined occupancy factors indicated a two third occupancy of the Cl site. At the same time a large thermal parameter indicated a high degree of disorder. Fourier maps did not reveal any splitting of the Cl site, putting an upper limit to a splitting to about 0.8 Å based on the $\sin\theta/\lambda$ resolution. To model a split Cl-site, the *y*-coordinate was varied manually in steps of 0.02, while the rest of the structure, including the thermal parameter of Cl was refined. Independent of radiation source and sample heat treatment all sets of refinements show a minimum in the thermal parameter when the *y*-coordinate of the Cl site was shifted 0.11 fractional units along the *b*-axis. Plots of the thermal parameter vs. *y*-coordinate of the Cl site are shown in Fig. 2 (left). The correct Cl site is thus suggested at (0,0.11,0) with a site occupancy factor of 2/3. The shortest Cl–Cl distance will then be 3.7 Å, Fig. 2 (right). In addition, the occupation must be at random as there are no evidence of a triple *b*-axis. This randomisation will be achieved with a few additional (random) vacancies. The approximately 1/3 Cl vacant sites will then be at a distance of 2.7 Å from a Cl site. Reducing this number by the ionic radius of Cl leaves a radius of 0.9 Å, which is far less than for example the radius of oxygen, 1.4 Å. It is therefore believed that the 1/3 Cl vacancies are really vacant.

From the H-akaganéite neutron diffraction study it was possible to locate and refine two fully occupied hydrogen sites, H1 and H3, bonded to O1 and O3, respectively. Each of the hydrogen is hydrogen bonded to chlorine. The refined H1 and H3 positions are slightly off the mirror plane at $y = 0$, consistent with the off-zero *y*-coordinate of the Cl site. The shortest hydrogen to framework oxygen distance, 2.9 Å, is too long to be considered a hydrogen bond interaction. The Fe–O1 and Fe–O3 distances are the longest Fe–O distances, consistent with them representing hydroxyl groups (Table 1).

Adding chloride ions to the FeO(OH) framework will require some charge balancing. It can be achieved by removing a corresponding amount of hydroxide ions

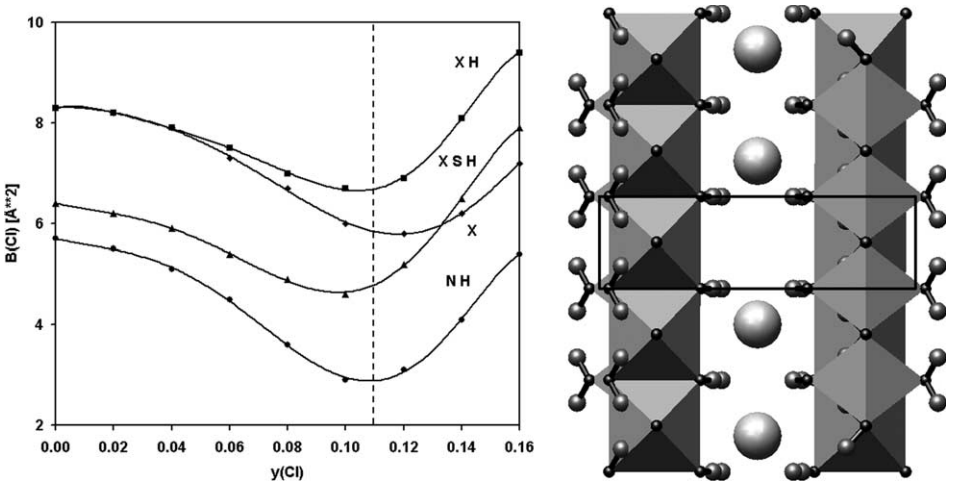


Fig. 2. Left: Chloride thermal parameter vs. $y$-coordinate from different powder diffraction experiments: X: conventional X-ray data, as-synthesized; XH: conventional X-ray data, sample heated to 175 °C for 1 h; X(S)H: synchrotron X-ray data, sample heated to 150 °C for 2 h; NH: neutron data, sample heated to 150 °C for 1 h. Right: Local ordering of chloride ions in 1/2, 1/2 ± 0.11, 1/2.

Table 1
Selected bonding distances (Å) in akaganéite for samples I and IV

| | | | | | |
|---|---|---|---|---|---|
| Fe(1) – O(1) [×2] | I | 2.20(1) | Fe(2) – O(2) | I | 1.99(2) |
| | IV | 2.10(1) | | IV | 1.97(2) |
| Fe(1) – O(1) | I | 2.05(1) | Fe(2) – O(3) [×2] | I | 2.10(2) |
| | IV | 2.29(2) | | IV | 2.04(1) |
| Fe(1) – O(2) [×2] | I | 1.92(1) | Fe(2) – O(3) | I | 2.21(1) |
| | IV | 2.01(1) | | IV | 2.02(2) |
| Fe(1) – O(4) | I | 1.90(2) | Fe(2) – O(4) [×2] | I | 1.99(1) |
| | IV | 1.95(2) | | IV | 1.95(1) |
| Cl – Cl | I | 3.70 | | | |
| | IV | 3.72 | | | |
| O(1) – H(1) | IV | 0.86(4) | O(3) – H(3) | IV | 1.31(3) |
| H(1) – – – Cl | IV | 2.49 | H(3) – – – Cl | IV | 2.33 |
| O(2) – H(2) | IV | 0.96 | O(4) – H(4) | IV | 0.98 |
| H(2) – – – O(1) | IV | 2.20 | H(4) – – – O(3) | IV | 2.10 |

Multiplicities are given in brackets. Standard errors are given in parenthesis for bonds involving atoms with refined coordinates.

or by adding hydrogen ions. None of the oxygen sites showed evidence of reduced occupancy. Instead could two additional hydrogen sites be located in a final difference Fourier map, H2 bonded to O2 and H4 bonded to O4. They are both located along an octahedral edge in the main channel and hydrogen bonded to O1 and O3, respectively (Table 1). The refined occupancies, 0.08(5) and 0.18(5) are of the right order of magnitude to fulfil the charge balancing in view of their relatively high

standard errors, but it was not possible to refine their coordinates. It was not possible to locate any residual density in the narrow channels connected to O2, as suggested for the extra hydrogen site by Post and Buchwald [19]. Neither was it possible to locate any hydrogen positions that would correspond to water hydrogens close to the vacant Cl sites. The chemical composition of akaganéite written to reflect the hydrogen positions would then be $FeO_{0.833}(OH)_{1.167}Cl_{0.167}$. The neutron powder diffraction pattern and the final Rietveld fit is shown in Fig. 3.

Akaganéite crystals are always very small. Depending on growth conditions, crystals are typically between 0.1 and 1 μm in the 0 1 0 (channel) direction and 0.01–0.1 μm in width (Cornell and Schwertmann [22]). The X-ray powder patterns show consistent particle-size broadening, with average crystallite dimensions of 0.14 μm by 0.035 μm, as refined using a Voigt profile function (Table 2). The very small particle sizes impose some additional difficulties in the interpretation of the powder diffraction results: A crystallite size of 0.035 μm in the *a*- and *c*-directions corresponds to 35 unit cells only. By adding/removing or ordering/disordering of a single layer of chlorides on the crystallite surfaces will cause variations in the refined Cl occupancies by about 6%, which may well explain most of the observed variations (Table 3). The uncertainty is inversely related to the crystallite sizes and has to be considered when comparing samples of different origin and/or treated at different temperatures.

*Phase transitions*. Two phase transitions has been observed during the course of this study. The first was the FeOCl formation from D-akaganéite at 150 °C. The reason for this transition is not fully clear, but it is likely to be related to very small crystallite sizes and high contents of adsorbed chloride. It was not possible to reproduce this transition with H-akaganéite. Another factor was the low temperature, 150 °C. A higher temperature would have resulted in hematite formation as described below. The diffraction pattern from the as-synthesized D-akaganéite shows generally poor diffracting power with particle size broadening and a high level of

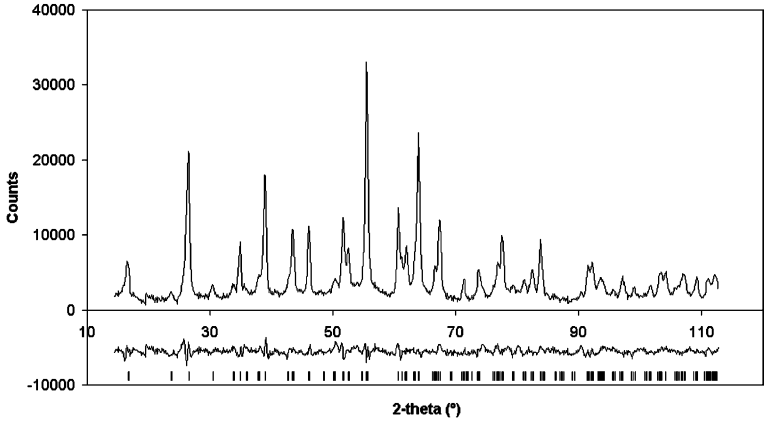


Fig. 3. Raw data and final difference plot after Rietveld refinements from neutron powder diffraction data of H-akaganéite pre-heated to 150 °C for 1 h. Vertical bars indicate Bragg positions.

Table 2
Powder diffraction data collection and refinement summary for akaganéite

| | Sample | | | |
|---|---|---|---|---|
| | I | II | III | IV |
| Sample treatment | As-synthesized | Heated to 175 °C for 1 h | Heated to 175 °C for 1 h and rehydrated | Heated to 150 °C for 1 h |
| Radiation | Conv. X-ray | Conv. X-ray | Conv. X-ray | Neutron |
| Wavelength (Å) | 1.54178 | 1.54178 | 1.54178 | 1.54172 |
| $2\theta$-range (°) | 15–130 | 15–130 | 15–130 | 9–113 |
| No. of Bragg reflections | 358 | 355 | 355 | 298 |
| No. of refined parameters | 37 | 36 | 36 | 40 |
| *Unit cell* | | | | |
| $a$ (Å) | 10.5536(7) | 10.4885(5) | 10.4878(8) | 10.612(2) |
| $b$ (Å) | 3.03449(8) | 3.0374(1) | 3.0381(1) | 3.0501(3) |
| $c$ (Å) | 10.5740(4) | 10.5088(5) | 10.5035(5) | 10.580(1) |
| $\beta$ (°) | 90.086(5) | 90.116(5) | 90.067(6) | 90.17(1) |
| Voigt particle size (Å) | 1210(39) × 366(8) | 1500(56) × 327(7) | 1438(32) × 358(8) | |
| $R_{\text{profile}}$ (%) | 8.61 | 9.92 | 10.48 | 8.29 |
| GOF | 1.96 | 2.17 | 2.53 | 4.37 |
| $R_{\text{Bragg}}$ (%) | 2.71 | 3.92 | 3.95 | 2.36 |

amorphous background scattering. It was not possible to perform any structure refinements from these data.

The second phase transition studied was the formation of hematite. The H-akaganéite samples were contained in glass capillaries and heated simultaneously as the powder diffraction patterns were recorded. A set of successively accumulated patterns is shown in a limited $2\theta$-range in Fig. 4. As seen, the transformation to hematite appears to start just above 200 °C and is rapidly completed at 250 °C. Repeating the experiment under apparently the same conditions do not always give exactly the same result in terms of transition temperature and completeness of reaction. Most likely does the amount and packing efficiency of the sample in the glass capillary together with particle size control the kinetics of the akaganéite to hematite reaction. However, neither of the diffraction pattern series showed any evidence for the formation of intermediate phases. Rietveld refinements of a set of successive powder patterns under transformation showed no consistent decrease of the chloride contents in the channels.

*TGA and MS analysis*. On heating akaganéite is loosing weight from about 50 °C and up to about 500 °C (Fig. 5). In a first step, 50–230 °C approximately 5% weight is lost. The MS signal indicates water loss only. This step can thus be attributed to loss of adsorbed water on the crystallite surfaces. At about 230 °C the weight loss increases abruptly. Based on the weight at 230 °C the weight loss in this second step is 16%. The abrupt weight loss is also connected with a rapid loss of chlorine as well as a continued loss of water as seen from the MS signals. Due to the length of the

Table 3
Fractional coordinates, and refined occupancy factors ($g$) for akaganéite

| | | Sample | | | |
|---|---|---|---|---|---|
| | | I | II | III | IV |
| Fe(1) | $x$ | 0.8578(5) | 0.8577(5) | 0.8604(6) | 0.8594(11) |
| | $z$ | 0.3455(3) | 0.3455(5) | 0.3487(4) | 0.3441(12) |
| Fe(2) | $x$ | 0.3426(6) | 0.3447(5) | 0.3433(6) | 0.3436(12) |
| | $z$ | 0.1451(4) | 0.1447(5) | 0.1452(5) | 0.1504(10) |
| O(1) | $x$ | 0.6679(13) | 0.6560(14) | 0.6730(15) | 0.6505(15) |
| | $z$ | 0.3034(10) | 0.2774(14) | 0.2913(12) | 0.2927(15) |
| O(2) | $x$ | 0.6722(15) | 0.6591(15) | 0.6560(17) | 0.6656(12) |
| | $z$ | 0.0471(12) | 0.0444(19) | 0.0336(15) | 0.0358(5) |
| O(3) | $x$ | 0.2874(14) | 0.3130(11) | 0.3171(17) | 0.2834(15) |
| | $z$ | 0.3514(10) | 0.3455(20) | 0.3570(14) | 0.3318(16) |
| O(4) | $x$ | 0.0372(15) | 0.0404(16) | 0.0440(20) | 0.0436(16) |
| | $z$ | 0.3402(11) | 0.3232(20) | 0.3271(13) | 0.3314(12) |
| Cl | $y$ | 0.11 | 0.11 | 0.11 | 0.11 |
| | $g$ | 0.201(2) | 0.166(3) | 0.156(3) | 0.194(7) |
| H(1) | $x$ | | | | 0.6134(24) |
| | $y$ | | | | 0.0844(51) |
| | $z$ | | | | 0.3621(34) |
| H(2) | $x$ | | | | 0.2810 |
| | $y$ | | | | 0.2340 |
| | $z$ | | | | 0.9350 |
| | $g$ | | | | 0.09(5) |
| H(3) | $x$ | | | | 0.3593(30) |
| | $y$ | | | | 0.0844(51) |
| | $z$ | | | | 0.4277(23) |
| H(4) | $x$ | | | | 0.0705 |
| | $y$ | | | | 0.2475 |
| | $z$ | | | | 0.2797 |
| | $g$ | | | | 0.18(5) |

Left out coordinates are all zero. Standard errors are given in parenthesis for refined parameters.

tubing (5 m) between the TG and MS equipment, the MS signal is somewhat delayed with respect to the TG signal. Some water will also condense in the tubing and dissolve some chlorine, which causes a further delay in the MS signal. Looking at the stoichiometry for the akaganéite to hematite reaction,

$$2FeO_{0.833}(OH)_{1.167}Cl_{0.167} \rightarrow Fe_2O_3 + 0.333HCl + H_2O$$

the expected weight loss is 15.9%, which is in excellent agreement with the observed weight loss.

*Mössbauer spectroscopy*. The Mössbauer spectrum recorded at 193 °C shows two major octahedral Fe(III) components contributing by approximately 42% each and a minor and broader octahedral component by approximately 13% (Fig. 6). These contributions are consistent with the two crystallographically different iron sites subject to a disorder due to the chlorine disorder. An additional quadruple doublet is probably an additional phase with a relative amount less than 3%.

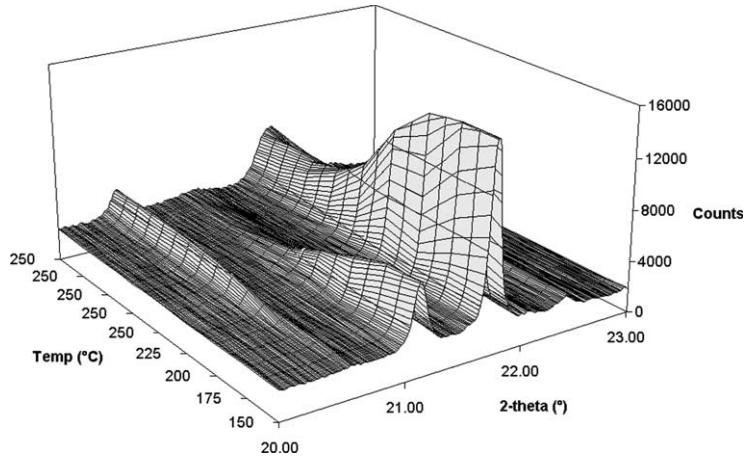


Fig. 4. In situ powder diffraction patterns showing the transformation from akaganéite to hematite.

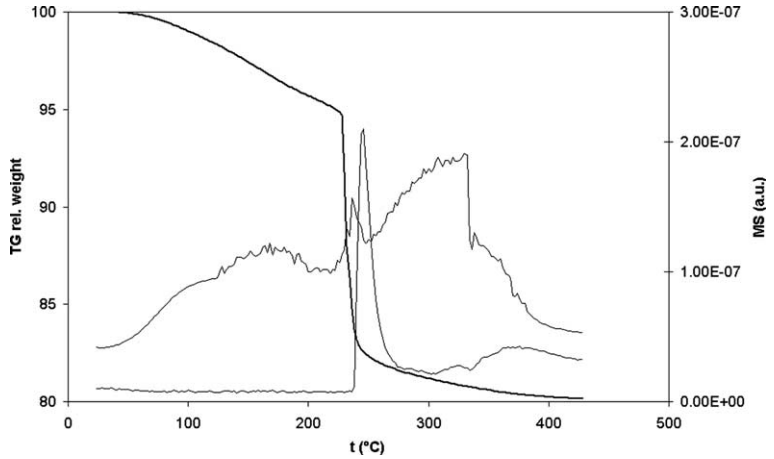


Fig. 5. TG and MS analysis for akaganéite. The TG curve (thick line) is scaled to give 100 at the starting position. The MS signals are in arbitrary units; lower curve—Cl and upper curve—$H_2O$.

## 4. Discussion

The crystal structure of akaganéite is similar to the hollandite structure, and can be described as being built from edge-and corner-sharing $Fe(O,OH)_6$ octahedra forming one-dimensional channels containing chloride ions. The chloride ions are distributed so as to occupy every two out of three of the formally possible sites. The chloride vacancies allows for a 0.33 Å displacement from the idealized 0,0,0 position resulting in realistic Cl–Cl distance of 3.72 Å. The vacant chloride sites are too close to the displaced chlorides to allow for water molecules simultaneously in the

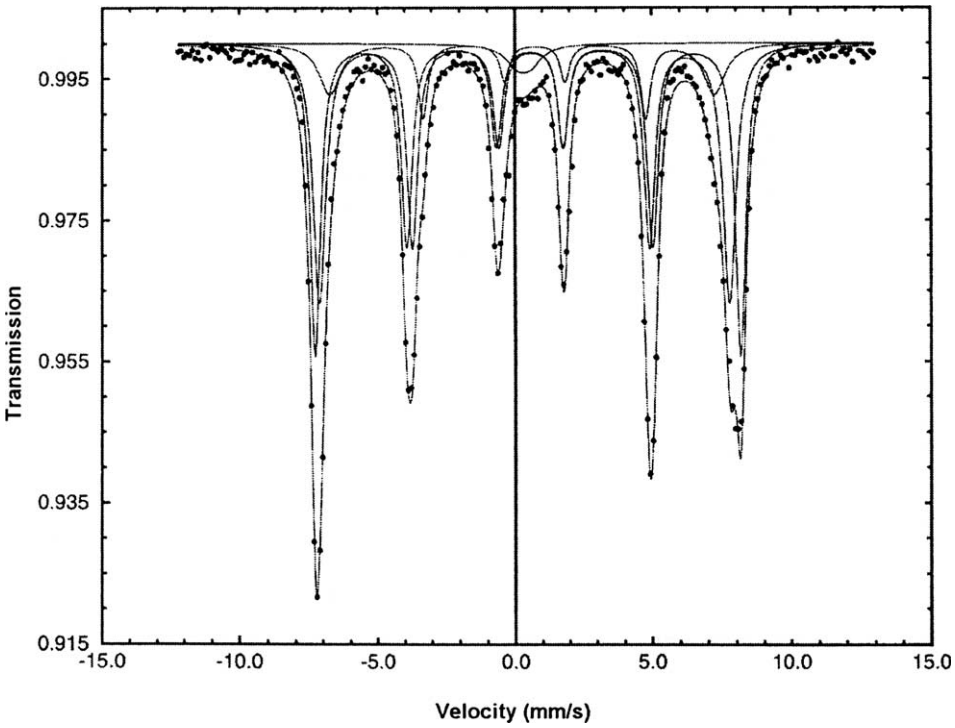


Fig. 6. Mössbauer spectrum of akaganéite collected at −193 °C. The lines show the fitted four individual Lorenzians as well as the total fit as compared to experimental points.

channels. Hydrogen appear in hydroxide groups, where the fully occupied hydrogen sites (H1 and H3) points into the channels forming hydrogen bonds to the chlorides. The partially occupied sites (H2 and H4) are found along octahedral edges and are hydrogen bonded to the opposite oxygen. The crystal structure is reflected in the tentative chemical formula for akaganéite:

$$FeO_{0.833}(OH)_{1.167}Cl_{0.167}$$

Mild heat treatment ($\leqslant 175$ °C) and rehydration does not change the crystal structure. Neither is the chloride contents significantly changed. The water loss (5%) registered below 230 °C in the TG analysis is entirely due to adsorbed water. The crystallite size is found to be in the order 0.14 μm by 0.035 μm, corresponding to only 10 unit cells in the *a*- and *c*-axes directions. The very small crystallite size seems to be an intrinsic property of akaganéite. The possibility of adsorption/desorption or ordering/disordering of surface layers thus requires a cautious interpretation of refined site occupancy factors.

The in situ powder diffraction and combined TGA–MS show only one phase transition, namely to hematite, when akaganéite is heated to 250 °C. There is no sign of chlorine release up to this transformation. Thus the release of chlorine is not a

prerequisite for the phase transition, but a mere consequence of it. The presence of chloride ions should be a critical factor for the build-up of the crystal structure from an acidic Fe(III) solution. The negative chloride ions will attract the positively charged $Fe(OH)_n(H_2O)_{(6-n)}^{(3-n)+}$ complexes in the acidic solution and will thereby act as a template for the channel formation. During synthesis, chlorides are locked into the akaganéite structure and cannot escape unless the structure is broken up.

## 5. Conclusion

The crystal structure of akaganéite has been firmly established by means of crystallography, TG, MS and Mössbauer spectroscopy. From a conservational perspective we can conclude that already present akaganéite should not as such posses a problem. Akaganéite will not transform or release chloride under normal conditions, i.e. temperatures below approximately 200 °C. Observations of chloride ion release on washing can be attributed to absorbed chloride ions on the large surface area of the intrinsically small akaganéite particles. When akaganéite transforms above 200 °C, it is to highly stable hematite with a specific volume smaller that that of akaganéite. While akaganéite as such is not a threat to iron artefacts, the formation of akaganéite from acidic chloride solutions on iron artefacts is a real problem. However, the solution to this problem is not primarily to remove akaganéite, but rather to remove the conditions leading to the formation of akaganéite. In other words, akaganéite is itself not a problem, but rather a symptom of a problem. It seems that conservation of archaeological iron will continue its search for better methods of stabilization, but that the "akaganéite phase" perhaps should be questioned.

## Acknowledgements

We are grateful to Ms G. Krarup, for performing the combined thermogravimetric and MS analyses, Ms L Berring and A. Schoneberg for synthesis and X-ray work, and the Danish Natural Science Research Council through DANSYNC for financial support.

## References

[1] S. Turgoose, Studies in Conservation 27 (1982) 97.
[2] S. Turgoose, in: R.W. Clarke, S.M. Blackshaw (Eds.), Maritime Monographs and Reports, no. 53. National Maritime Museum, 1982, p. 1.
[3] N.A. North, Studies in Conservation 27 (1982) 75.
[4] L.S. Selwyn, P.J. Sirois, V. Argyropoulos, Studies in Conservation 44 (1999) 217.
[5] F. Zucchi, G. Morigi, V. Bertolasi, Corrosion and Metal Artifacts, NBS Special Publication no. 479, Washington, 1977, pp. 103–105.
[6] A. Askey, S.B. Lyon, G.E. Thompson, J.B. Johnson, G.C. Wood, M. Cook, P. Sage, Corrosion Science 34 (1993) 233.

[7] R.F. Tylecote, J.W. Black, Studies in Conservation 25 (1980) 87.
[8] N.A. North, C. Pearson, Studies in Conservation 22 (1977) 146.
[9] P. Arnould-Pernot, C. Forrières, H. Michel, B. Weber, Studies in Conservation 39 (1993) 232.
[10] P. Arnould-Pernot, C. Forrières, H. Michel, B. Weber, Metal 95 in: I.D. MacLeod, S.L. Pennec, L. Robiolla (Eds.), James and James Ltd., London, 1997, 147.
[11] K. Schmidt-Ott, V. Boissonnas, Studies in Conservation 47 (2002) 81.
[12] D. Watkinson, Archaeological Conservation and its Consequences, IIC, Copenhagen, 1996, p. 208.
[13] C. Costain, Journal of the Canadian Association for Conservation 25 (2000) 11.
[14] S. Keene, in: D.A. Scott, J. Podany, B. Considine (Eds.), Ancient & Historic Metals: Conservation and Scientific Research, Getty Conservation Institute, 1991, p. 249.
[15] J. van Lanschot, T. Mathiesen, C.D. Szalkay, S. Turgoose, in: 4th International Conference, Non-Destructive Testing of Works of Art, Deutsche Gesellschaft für Zerstörungsfreie Prüfung, e.V. 45 Teil 1 (1994) 306.
[16] H.B. Weiser, W.O. Milligan, J. Am. Chem. Soc. 57 (1935) 238.
[17] A.L. Mackay, Mineral Magazine 32 (1960) 545.
[18] A.L. Mackay, Mineral Magazine 33 (1962) 270.
[19] J.E. Post, V.F. Buchwald, American Mineralogist 76 (1991) 272.
[20] P. Norby, J. Appl. Cryst. 30 (1997) 21.
[21] C.J. Howard, R.J. Hill, A computer program for Rietveld analysis of fixed X-ray and neutron powder diffraction patterns, AAEC (now ANSTO) Report M112, Lucas Heights Research Laboratory, Australia, 1986.
[22] R.M. Cornell, U. Schwertmann, The Iron Oxides, VCH, Weinheim, Germany, 1996.